Superdispersive plasmonic metamaterial

V.M. Muravev,[1,*] K.R. Dzhikirba,[1,2] M.S. Sokolova,[1,2] A.S. Astrakhantseva,[1,2] and I.V. Kukushkin[1]

[1] *Osipyan Institute of Solid State Physics, Russian Academy of Sciences (RAS), Chernogolovka, 142432 Russia*
[2] *Moscow Institute of Physics and Technology, Dolgoprudny, 141700 Russia*

(Received 8 December 2023; revised 3 February 2024; accepted 26 February 2024; published 20 March 2024)

We realize a simple technology to assemble a three-dimensional metamaterial consisting of stacked planar silicon chips with a metallic mesh lithographically fabricated on the chip surface. We use Fabry-Perot resonance spectroscopy to accurately measure the metamaterial dispersion in the terahertz frequency range. For large mesh periods, the dispersion closely follows the plasmonic dependence, with the plasma frequency determined by the geometric parameters of the metamaterial. For small mesh periods, the dispersion gains extreme sensitivity to the radiation frequency. Such a superdispersive property may have implications in the field of spectroscopy and multiplexing.

DOI: 10.1103/PhysRevApplied.21.034041

I. INTRODUCTION

Periodic metallic structures have the ability to simulate various homogeneous materials the specific properties of which eventually do not exist for natural materials. For example, when its characteristic dimensions are small in comparison to the wavelength, a three-dimensional (3D) periodic mesh of metallic thin wires behaves as a homogenous metamaterial with a plasma frequency [1,2] of

$$\omega_p^2 = \frac{2\pi c^2}{a^2 \ln(a/r)}. \tag{1}$$

Here, a is the array lattice constant and r is the radius of the wires. Thus, the metamaterial exhibits a highly dispersive nature with $\varepsilon(\omega) = 1 - \omega_p^2/\omega^2$. Experimentally, the expression given in Eq. (1) has been verified roughly using the electromagnetic transparency of the plasmonic metamaterials above the plasma frequency [3–5].

Initially, plasmonic metamaterials have been used to create various microwave quasioptical elements (lenses, prisms, and holograms) [6–9]. After a few decades, attention to metamaterials has returned in the wake of new ideas related to left-handed metamaterials. Since the original work in 1968 [10], left-handed metamaterials have demonstrated many unconventional physical properties [11–13]. More recently, plasmonic metamaterials have opened up another interesting area of epsilon-near-zero (ENZ) materials [14,15]. The ENZ metamaterials have already shown interesting implications in the fields of supercoupling [16, 17], nonlinear optics [18–20], and directive emission [21]. Despite promising prospects, the development of metamaterials is severely slowed down by the challenges in synthesis and their high internal absorption.

In the present paper, we propose and realize a simple technology to assemble a 3D plasmonic metamaterial from a stack of silicon chips with metallic mesh lithographically produced on their surface [22]. We use spectroscopy of Fabry-Perot resonances for the accurate measurement of the metamaterial dispersion, $\varepsilon(\omega) = \varepsilon\,(1 - \omega_p^2/\omega^2)$. It turns out that the plasma frequency is described quite accurately by the expression (see the Supplemental Material [23])

$$\omega_p^2 = \frac{2\pi c^2}{\varepsilon\, ad\, \ln(a/w)}, \quad \omega_p \ll \frac{c}{\sqrt{\varepsilon} d}, \tag{2}$$

where $\varepsilon = 11.9$ is the dielectric constant of silicon, a is a mesh period, w is the mesh width, and d is the thickness of the chip. Most importantly, we have found that when the plasmon frequency ω_p reaches the stop-band edge, the effective dielectric permittivity of the metamaterial gains extreme sensitivity to the radiation frequency. Such a superdispersive property can find important implications in the field of terahertz spectroscopy and spatial multiplexing [24–26].

II. EXPERIMENTAL METHOD

The metamaterial samples under study have been constructed from high-resistivity $> 30\ \mathrm{k\Omega} \times$ cm silicon chips with dimensions of 1×1 cm^2. We have measured two series of samples with chip thicknesses of $d = 105$ and 210 μm. A metallic mesh with a period $a = 0.1 - 0.3$ mm

*muravev@issp.ac.ru

and a strip width $w = 5 - 30$ μm is lithographically fabricated on one side of each semiconductor chip. The metallic layer, which contains Cr (25 nm) and Au (700 nm), is thermally evaporated in a vacuum chamber. The thickness of the metallization has been chosen to be thicker than the skin layer at a typical experimental frequency $\delta(100\ \text{GHz}) = 250$ nm. The silicon chips are aligned and pressed tightly to form a resulting metamaterial [Fig. 1(a)]. It has been shown that the electrodynamic properties of the devised metamaterial are robust with respect to the alignment of the mesh structures and small defects in the metamaterial (see the Supplemental Material [23]). The direction of the electric field in the incident electromagnetic wave is shown in Fig. 1(a) by the red arrow. The metamaterial sample is mounted across the optical path of the terahertz beam. We employ a set of backward-wave oscillators (BWOs) covering the frequency range of 50–400 GHz as a source of continuous terahertz radiation. The electromagnetic radiation from the source is directed normally to the sample surface. The transmitted power is synchronously detected with a pyroelectric detector at a modulation frequency of 1 kHz. Further technical details on the setup and procedure used in the terahertz quasioptic experiment can be found elsewhere [27].

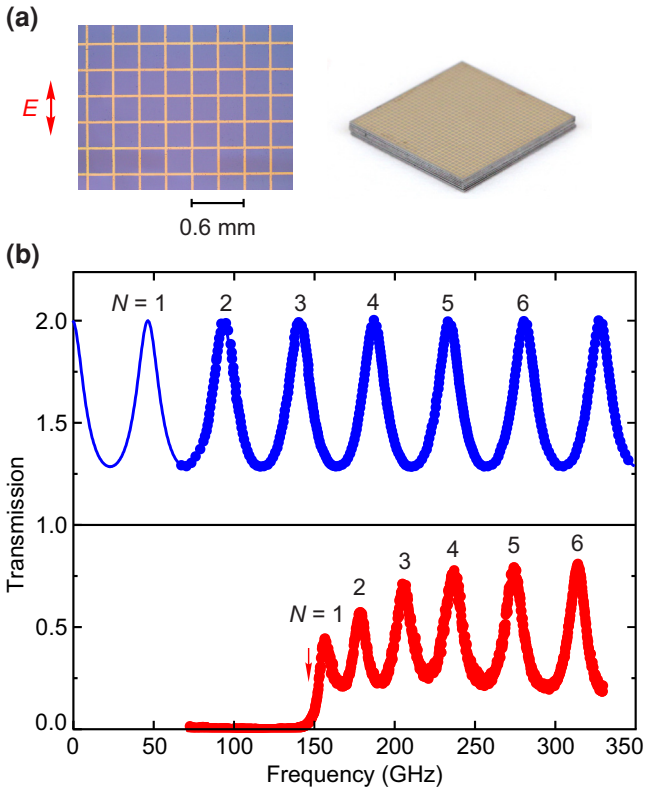

FIG. 1. (a) Left: a single silicon chip with a metallic mesh on the surface ($a = 0.3$ mm, $w = 30$ μm). Right: a side view of the metamaterial stack containing nine chips. (b) Top: the transmission spectrum measured for the stack of nine silicon chips with a total thickness of $h = 0.95$ mm. Bottom: the transmission spectrum measured for the same stack of nine silicon chips with a metallic mesh lithographically fabricated on the surface of each substrate. The mesh has a period $a = 0.2$ mm and the width of the metal strips $w = 10$ μm. The arrow marks the frequency of the plasma edge $f_p = 146$ GHz.

III. EXPERIMENTAL RESULTS

The red dots in Fig. 1(b) display the transmission through the metamaterial sample containing nine chips. The lattice on each chip has a period $a = 0.2$ mm and a strip width of $w = 10$ μm. The measured transmission curve has two interesting features. First, the plasma edge is clearly distinguishable at the frequency $f_p = 146$ GHz [arrow in Fig. 1(b)]. Below the plasma frequency, the transmission of the metamaterial is virtually zero. Above the plasma frequency, the transmission demonstrates a set of Fabry-Perot resonances. The sequence of these resonances differs dramatically from that of an empty Si substrate with the same thickness [blue dots in Fig. 1(b)]. The Fabry-Perot resonances are spaced nonequidistantly on the frequency scale due to the highly dispersive nature of the designed metamaterial. Also, the first $N = 1$ Fabry-Perot resonance shows a substantial shift from 47 GHz up to 157 GHz, indicating that the effective dielectric constant of the metamaterial is much lower than that of the bulk silicon $\varepsilon = 11.9$.

Using the frequency position of the successive Fabry-Perot modes, one can study the dispersive properties of the metamaterial. Such a Fabry-Perot ethalon method has been widely used to study the dispersion of different excitations, e.g., exciton polaritons [28,29] and plasmons [30]. In Fig. 2(a), we display transmission spectra recorded for the metamaterial stack assembled from a different number of layers. The curves are offset vertically by one unit for clarity. Each Fabry-Perot resonance has been assigned a sequential number $N = 1, 2, 3, \ldots$ The dotted lines in Fig. 2(a) serve as a guide for the eye, linking the peaks with $N = 1$, 2, 3, and 4 as they disperse with increasing stack number. It is interesting to note that a broad resonance on metamaterial containing a single chip corresponds to the excitation of a $N = 0$ Fabry-Perot mode. The shift of this resonance from zero frequency is due to plasma effects. A detailed description of this phenomenon is given elsewhere [31–34], and we will not discuss it in this paper.

The Fabry-Perot resonance frequency is determined by the standard expression

$$\omega_N = N\frac{\pi}{h}\frac{c}{\sqrt{\varepsilon(\omega)}}, \quad \varepsilon(\omega) = \left(N\frac{\pi}{h}\frac{c}{\omega_N}\right)^2, \qquad (3)$$

where h is the total thickness of the metamaterial. The resultant effective permittivity $\varepsilon(\omega)$ of the metamaterial under study is summarized in Fig. 2(b). It is very well described by the plasma relation $\varepsilon(\omega) = \varepsilon(1 -$

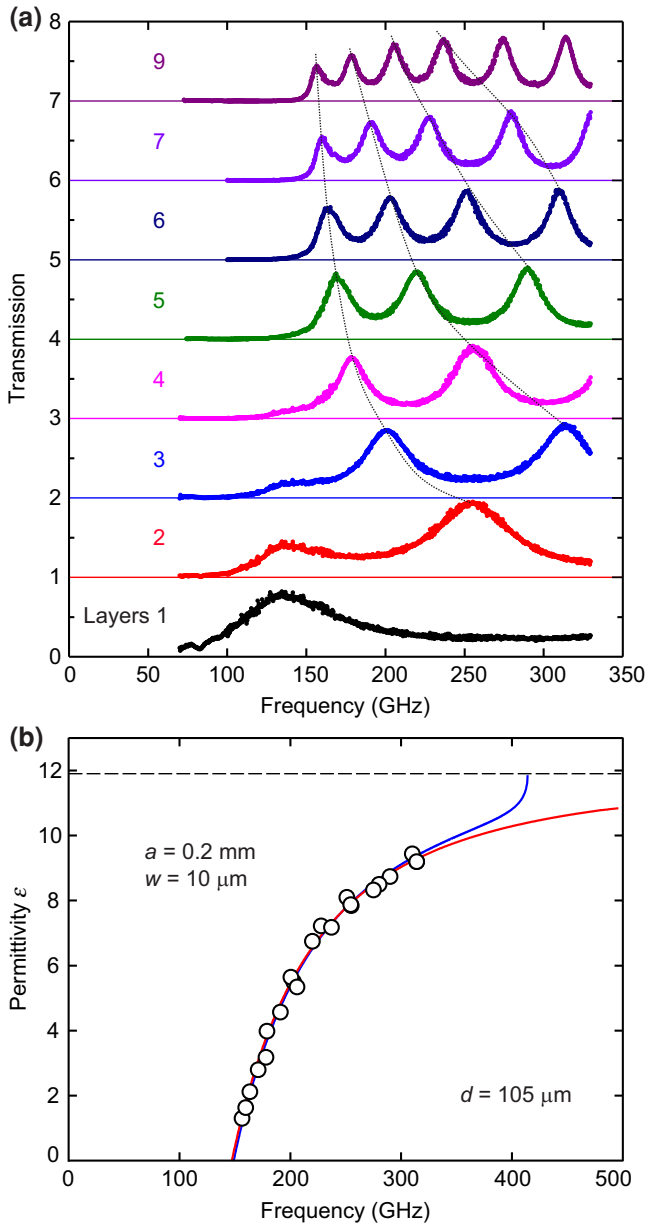

FIG. 2. (a) Transmission spectra measured for the plasmonic metamaterial with different numbers of chips in the stack. Each chip has a thickness of $d = 105$ μm and mesh geometric dimensions of $a = 0.2$ mm and $w = 10$ μm. The dotted lines serve as a guide for the eye, linking the peaks with $N = 1$, 2, 3, and 4 as they disperse with increasing stack number. (b) The dispersion $\varepsilon(\omega)$ of the electromagnetic wave traveling through the metamaterial. The different points correspond to distinct Fabry-Perot resonances. The red line depicts the relation $\varepsilon(\omega) = \varepsilon\,(1 - \omega_p^2/\omega^2)$ with the plasma frequency $f_p = \omega_p/2\pi = 146$ GHz. The blue line shows the dispersion calculated from Eq. (4), taking photonic crystal effects into account. The dashed horizontal line denotes the bulk permittivity of the silicon (Si).

ω_p^2/ω^2) with the plasma frequency $f_p = 146$ GHz [red line in Fig. 2(b)]. Therefore, the metamaterial under study exhibits all of the physical properties of the 3D plasma. In these considerations, we have neglected the attenuation in the metamaterial. We believe that this is justified by the fact that, according to experimental data from Fig. 2(a), the transmission of the metamaterial samples is rather high. Indeed, the transmission at the Fabry-Perot maxima equals 0.8 for the thickest sample with nine chips in the stack.

To further study the plasmonic properties of the metamaterial, we have performed the same experimental sets with metamaterials having chip thicknesses $d = 105$ and 210 μm and mesh geometrical parameters $a = 0.3$, 0.2, and 0.1 mm and $w = 5$, 10, and 30 μm. For each metamaterial configuration, we carefully determined the plasma frequency. The resultant dependencies of the plasma frequency on the geometrical parameters are presented in Fig. 3. The solid lines in Fig. 3 are according to Eq. (2). There is a surprisingly good agreement between the experimental data and the theoretical formula for the plasma frequency.

The metamaterial concept only works well if the radiation wavelength is much larger than the characteristic scale of the material. In our case, this translates into two conditions: $a \ll \lambda/\sqrt{\varepsilon}$ and $d \ll \lambda/\sqrt{\varepsilon}$. In the case of $a \geq \lambda/\sqrt{\varepsilon}$, the diffraction scattering of the incident electromagnetic wave begins to play a major role (see Supplemental Material [23] for experimental demonstration). In turn, the failure of the second condition ($d \ll \lambda/\sqrt{\varepsilon}$) results in photonic crystal effects [35]. It turns out that the photonic crystal effects, in conjunction with the plasmonic properties, lead to interesting physical implications.

The expression $\varepsilon(\omega) = \varepsilon\,(1 - \omega_p^2/\omega^2)$ naturally stops working at large d or high frequencies. An advanced analysis yields the following expression for the dispersion of the wave traveling in the mesh medium [8,9]:

$$\cos\left(\frac{\omega}{c}d\sqrt{\varepsilon(\omega)}\right) = \cos\left(\frac{\omega}{c}d\sqrt{\varepsilon}\right) + \frac{\pi c}{\sqrt{\varepsilon}\,\omega a \ln(a/w)}\sin\left(\frac{\omega}{c}d\sqrt{\varepsilon}\right). \tag{4}$$

The resultant dispersion calculated for the plasmonic metamaterial with $a = 0.2$ mm and $w = 10$ μm is shown by the blue curve in Fig. 2(b). There is a noticeable deviation from the plasma dispersion (red curve) starting from the frequency of 300 GHz. An important consequence of Eq. (4) is that it predicts the emergence of the first photonic stop band above the frequency:

$$\omega_{sb} = \frac{c}{\sqrt{\varepsilon}}\frac{\pi}{d}, \tag{5}$$

which is equivalent to $d = \lambda_{sb}/2\sqrt{\varepsilon}$. It is interesting that at the stop-band frequency, the effective dielectric permittivity of the metamaterial $\varepsilon(\omega_{sb}) = \varepsilon$. In particular, for the metamaterial under consideration with the chip thickness $d = 105$ μm, this gives $f_{sb} = 414$ GHz.

To further investigate the interplay between plasmonic and photonic crystal effects, we have assembled

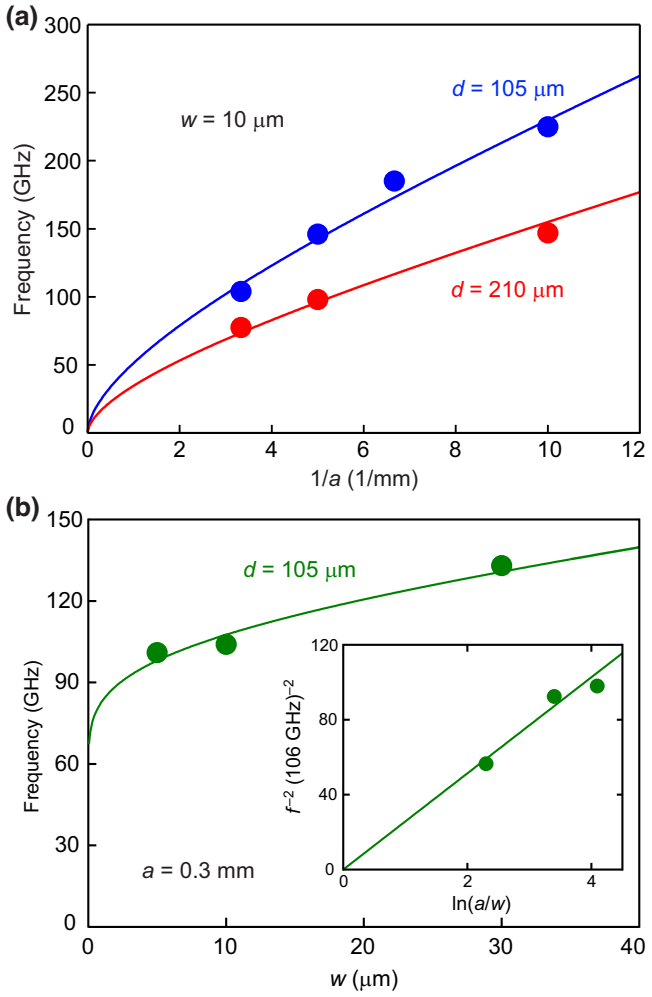

FIG. 3. (a) The experimental dependence of the plasma frequency on the inverse period of the mesh, $1/a$. The experiments have been carried out for two batches of samples with an individual chip thickness $d = 105$ (blue dots) and 210 μm (red dots). (b) The plasma frequency versus the strip width, w. The inset shows the same data on the f^{-2} versus $\ln(a/w)$ axis. The solid lines demonstrate the theoretical prediction according to Eq. (2).

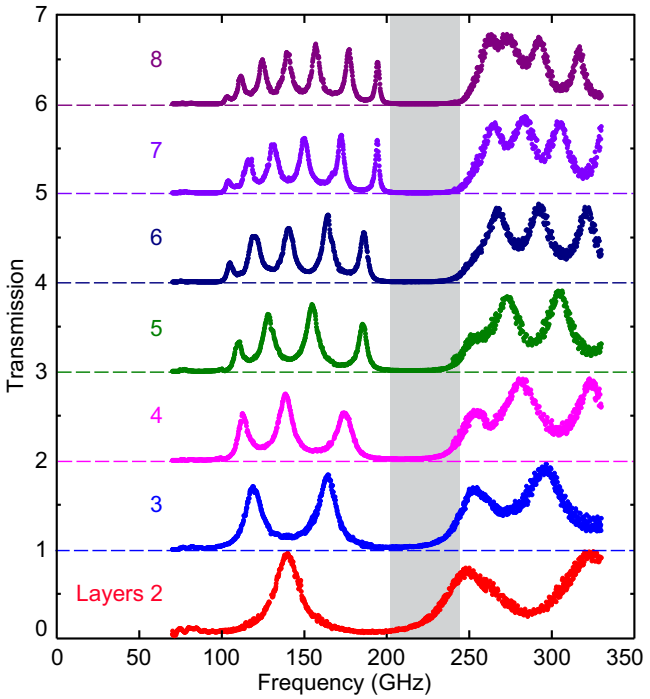

FIG. 4. Transmission spectra measured for the plasmonic metamaterial with different numbers of chips in the stack. Each chip has a thickness $d = 210$ μm and mesh geometric dimensions of $a = 0.2$ mm and $w = 10$ μm. The gray area represents the region of the photonic stop band.

metamaterials from the thicker silicon slabs with $d = 210$ μm. The transmission spectra measured for such plasmonic metamaterial stacks with a period $a = 0.2$ mm and a width of strips $w = 10$ μm are shown in Fig. 4. The transmission curves for metamaterials with different numbers of layers are offset vertically by one unit. In fact, a nontransparent stop band appears starting from $N = 5$ layers in the frequency range from 200 up to 245 GHz. The stop-band edge of 200 GHz agrees well with the predicted $f_{sb} = 207$ GHz. In Fig. 5, we depict the dispersion, $\varepsilon(f)$, measured for a series of metamaterials with different lattice periods $a = 0.3$, 0.2 and 0.1 mm but with a fixed chip thickness $d = 210$ μm and a strip width $w = 10$ μm. The obtained $\varepsilon(f)$ dependencies deviate strongly from those of the simple plasmonic model, $\varepsilon(\omega) = \varepsilon\,(1 - \omega_p^2/\omega^2)$ (dashed lines in Fig. 5). On the other hand, the more elaborate approach given in Eq. (4) works quite well (solid lines in Fig. 5).

In the plasmonic metamaterial, the electromagnetic wave is only allowed to propagate in the frequency range between the plasma and the stop-band edge. If the plasma frequency, f_p, is close to the edge of the stop band, f_{sb}, then the metamaterial demonstrates extremely large dispersion $\partial\varepsilon/\partial f$. Indeed, the average dispersion for the plasmonic metamaterial with $a = 0.1$ mm from Fig. 5 equals $\partial\varepsilon/\partial f = 0.18$ GHz^{-1}. For comparison, the dispersion of light in borosilicate crown glass is $\partial\varepsilon/\partial f = 1.69 \cdot 10^{-7}$ GHz^{-1} (for more details, see the Supplemental Material [23]). The black curve in Fig. 5 contains a dispersive region from 75 up to 125 GHz and another region from 125 to 200 GHz where the permittivity variation flattens out with respect to the frequency. This will certainly complicate the use of the dispersive behavior for spectroscopy. On the other hand, the red curve in Fig. 5 displays an almost linear permittivity variation in frequency over the entire usable bandwidth of 140–200 GHz or, equivalently, a relatively constant large dispersion. This is extremely useful for spectroscopy, as a linear change in frequency would translate into a relatively linear position shift of the beam. However, achieving this behavior requires engineering ω_p and ω_{sb} so that they are close in frequency. This, in turn,

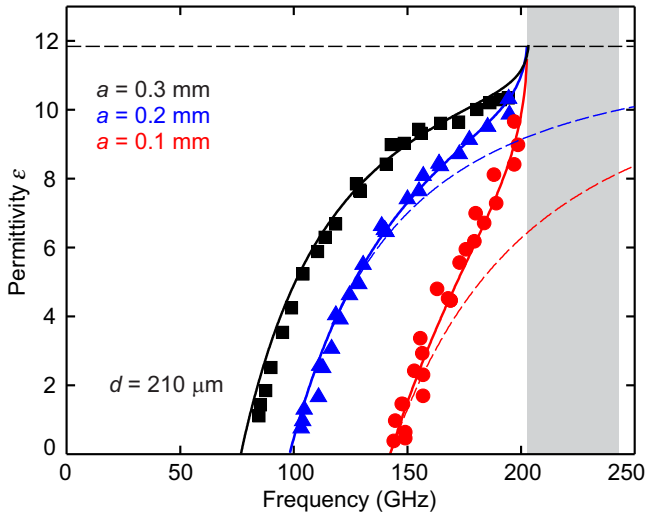

FIG. 5. The dielectric permittivity of the plasmonic metamaterial with a chip thickness $d = 210$ μm, measured for silicon chips with different lattice constants $a = 0.1$, 0.2, and 0.3 mm. The strip width has been fixed to $w = 10$ μm. The dashed and solid lines illustrate the results of the theoretical model given in Eqs. (2) and (4), respectively. The gray area represents the region of the photonic stop band.

drastically limits the available bandwidth of the superdispersive character, implying a trade-off between the value of the dispersion and the transparency bandwidth.

The observed superdispersive effect can be used to realize a "superprism phenomenon" [36]. A prism made from the plasmonic metamaterial will lead to an extremely large angular dispersion. The ability of the superprism to direct beams with varying wavelengths to significantly different angles in space has potential applications in spectroscopy and wavelength demultiplexing. The spectroscopy of the incident radiation can be performed by a spatial decomposition of the incident beam by the superprism, with subsequent detection by a linear terahertz camera [37,38]. In turn, wavelength demultiplexing may be used for a radar system, where the oscillator frequency swing implements the beam steering.

IV. CONCLUSIONS

In conclusion, we have fabricated and studied 3D metamaterial assembled from silicon chips with metallic mesh on the chip surfaces. We have found out that the electrodynamic response of the metamaterial can be described in terms of the effective dielectric permittivity. For large mesh periods, the dispersion of the electromagnetic wave traveling through the metamaterial closely follows the plasmonic dependency, with the plasma frequency determined by the geometric parameters of the mesh and the chip thickness. In another limit, when the mesh period is small, the metamaterial demonstrates extremely large dispersion, $\partial\varepsilon/\partial f$. The superdispersive effect has proved to be robust with respect to the alignment of the mesh structures and small defects in the metamaterial (see the Supplemental Material [23,39]). The superdispersive property that we have discovered may have implications in the field of terahertz spectroscopy and multiplexing.

ACKNOWLEDGMENTS

We gratefully acknowledge the financial support from the Russian Science Foundation (Grant No. 19-72-30003). We are also grateful to P. A. Gusikhin for the simulation results included in the online Supplemental Material [23].

[1] W. Rotman, Plasma simulation by artificial dielectrics and parallel-plate media, IRE Trans. Antennas Propag. **10**, 17 (1962).
[2] J. B. Pendry, A. J. Holden, W. J. Stewart, and I. Youngs, Extremely low frequency plasmons in metallic mesostructures, Phys. Rev. Lett. **76**, 4773 (1996).
[3] J. B. Pendry, A. J. Holden, D. J. Robbins, and W. J. Stewart, Low frequency plasmons in thin-wire structures, J. Phys.: Condens. Matter **10**, 4785 (1998).
[4] D. R. Smith, D. C. Vier, W. Padilla, S. C. Nemat-Nasser, and S. Schultz, Loop-wire medium for investigating plasmons at microwave frequencies, Appl. Phys. Lett. **75**, 1425 (1999).
[5] P. Gay-Balmaz, C. Maccio, and J. F. Martin, Microwire arrays with plasmonic response at microwave frequencies, Appl. Phys. Lett. **81**, 2896 (2002).
[6] W. E. Kock, Metallic delay lenses, Bell Syst. Tech. J. **27**, 58 (1948).
[7] S. S. D. Jones and J. Brown, Metallic delay lenses, Nature **163**, 324 (1949).
[8] J. Brown, The design of metallic delay dielectrics, Proc. IEE **97**, 45 (1950).
[9] J. Brown, Artificial dielectrics having refractive indices less than unity, Proc. IEEE **100**, 51 (1953).
[10] V. G. Veselago, The electrodynamics of substances with simultaneously negative values of ε and μ, Sov. Phys. Usp. **10**, 509 (1968).
[11] D. R. Smith, W. J. Padilla, D. C. Vier, S. C. Nemat-Nasser, and S. Schultz, Composite medium with simultaneously negative permeability and permittivity, Phys. Rev. Lett. **84**, 4184 (2000).
[12] R. A. Shelby, D. R. Smith, S. C. Nemat-Nasser, and S. Schultz, Microwave transmission through a two-dimensional, isotropic, left-handed metamaterial, Appl. Phys. Lett. **78**, 489 (2001).
[13] R. A. Shelby, D. R. Smith, and S. Schultz, Experimental verification of a negative index of refraction, Science **77**, 292 (2001).
[14] N. Engheta, Pursuing near-zero response, Science **340**, 286 (2013).
[15] I. Liberal and N. Engheta, Near-zero refractive index photonics, Nat. Photonics **11**, 149 (2017).

[16] M. G. Silveirinha and N. Engheta, Tunneling of electromagnetic energy through subwavelength channels and bends using ε-near-zero materials, Phys. Rev. Lett. **97**, 157403 (2006).

[17] B. Edwards, A. Alù, M. E. Young, M. Silveirinha, and N. Engheta, Experimental verification of epsilon-near-zero metamaterial coupling and energy squeezing using a microwave waveguide, Phys. Rev. Lett. **100**, 033903 (2008).

[18] M. Z. Alam, I. De Leon, and R. W. Boyd, Large optical nonlinearity of indium tin oxide in its epsilon-near-zero region, Science **352**, 795 (2016).

[19] L. Caspani, R. P. M. Kaipurath, M. Clerici, M. Ferrera, T. Roger, J. Kim, N. Kinsey, M. Pietrzyk, A. Di Falco, V. M. Shalaev, A. Boltasseva, and D. Faccio, Enhanced nonlinear refractive index in ε-near-zero materials, Phys. Rev. Lett. **116**, 233901 (2016).

[20] M. Z. Alam, S. A. Schulz, J. Upham, I. De Leon, and R. W. Boyd, Large optical nonlinearity of nanoantennas coupled to an epsilon-near-zero material, Nat. Photonics **12**, 79 (2018).

[21] S. Enoch, G. Tayeb, P. Sabouroux, N. Guérin, and P. Vincent, A metamaterial for directive emission, Phys. Rev. Lett. **89**, 213902 (2002).

[22] C. A. M. Butler, J. Parsons, J. R. Sambles, A. P. Hibbins, and P. A. Hobson, Microwave transmissivity of a metamaterial-dielectric stack, Appl. Phys. Lett. **95**, 174101 (2009).

[23] See the Supplemental Material at http://link.aps.org/supplemental/10.1103/PhysRevApplied.21.034041 for the following topics: derivation of the formula for the metamaterial plasma frequency; the applicability of the effective medium concept; the sensitivity of the metamaterial properties to the alignment of the mesh structures; the effect of the metal-mesh thickness; and a comparison of the dispersions of glass and the engineered plasmonic metamaterial.

[24] H. Xing, J. Fan, D. Lu, Z. Gao, P. P. Shum, and L. Cong, Terahertz metamaterials for free-space and on-chip applications: From active metadevices to topological photonic crystals, Adv. Dev. Instrum. **2022**, 9852503 (2022).

[25] I. Aupiais, R. Grasset, T. Guo, D. Daineka, J. Briatico, S. Houver, L. Perfetti, J.-P. Hugonin, J.-J. Greffet, and Y. Laplace, Ultrasmall and tunable terahertz surface plasmon cavities at the ultimate plasmonic limit, Nat. Commun. **14**, 7645 (2023).

[26] V. Cecconi, V. Kumar, J. Bertolotti, L. Peters, A. Cutrona, L. Olivieri, A. Pasquazi, J. Sebastian, T. Gongora, and M. Peccianti, Terahertz spatiotemporal wave synthesis in random systems, ACS Photonics **11**, 362 (2024).

[27] G. Kozlov and A. Volkov, *Millimeter and submillimeter Wave Spectroscopy of Solids*, edited by G. Gruner (Springer Berlin Heidelberg, 1998), Vol. 74.

[28] V. A. Kiselev, B. S. Razbirin, and I. N. Uraltsev, Additional waves and Fabry-Perot interference of photoexcitons (polaritons) in thin II–VI crystals, Phys. Stat. Solidi B **72**, 161 (1975).

[29] J. Voigt, M. Senoner, and I. Ruckmann, Quantitative analysis of interference structures in the transmission spectrum of very thin CdS platelets, Phys. Stat. Solidi B **75**, 213 (1976).

[30] A. M. Zarezin, P. A. Gusikhin, V. M. Muravev, and I. V. Kukushkin, Spectra of two-dimensional proximity plasmons measured by the standing-wave method, JETP Lett. **111**, 282 (2020).

[31] Yu. A. Kosevich, Total transmission of electromagnetic waves and homogeneous plasma resonance of 2D electron gas, JETP Lett. **53**, 150 (1991).

[32] P. A. Gusikhin, V. M. Muravev, and I. V. Kukushkin, Superluminal electromagnetic two-dimensional plasma waves, Phys. Rev. B **102**, 121404(R) (2020).

[33] A. Shuvaev, V. M. Muravev, P. A. Gusikhin, J. Gospodarič, A. Pimenov, and I. V. Kukushkin, Discovery of two-dimensional electromagnetic plasma waves, Phys. Rev. Lett. **126**, 136801 (2021).

[34] A. S. Astrakhantseva, A. Shuvaev, P. A. Gusikhin, A. Pimenov, I. V. Kukushkin, and V. M. Muravev, Terahertz plasma edge engineering in semiconductor membranes with a two-dimensional electron layer, Appl. Phys. Lett. **120**, 031104 (2022).

[35] J. D. Joannopoulos, P. R. Villeneuve, and S. Fan, Photonic crystals, Solid State Commun. **102**, 165 (1997).

[36] H. Kosaka, T. Kawashima, A. Tomita, M. Notomi, T. Tamamura, T. Sato, and S. Kawakami, Superprism phenomena in photonic crystals, Phys. Rev. B **58**, R10096(R) (1998).

[37] A. V. Shchepetilnikov, P. A. Gusikhin, V. M. Muravev, G. E. Tsydynzhapov, Yu. A. Nefyodov, A. A. Dremin, and I. V. Kukushkin, New ultra-fast sub-terahertz linear scanner for postal security screening, J. Infrared Millim. Terahertz Waves **41**, 655 (2020).

[38] A. V. Shchepetilnikov, P. A. Gusikhin, V. M. Muravev, B. D. Kaysin, G. E. Tsydynzhapov, A. A. Dremin, and I. V. Kukushkin, Linear scanning system for THz imaging, Appl. Opt. **60**, 10448 (2021).

[39] G. G. Macfarlane, Surface impedance of an infinite parallel-wire grid at oblique angles of incidence, J. IEE **93**, 1523 (1946).